iScience

CellPress
OPEN ACCESS

Article

Defects of renal tubular homeostasis and cystogenesis in the *Pkhd1* knockout

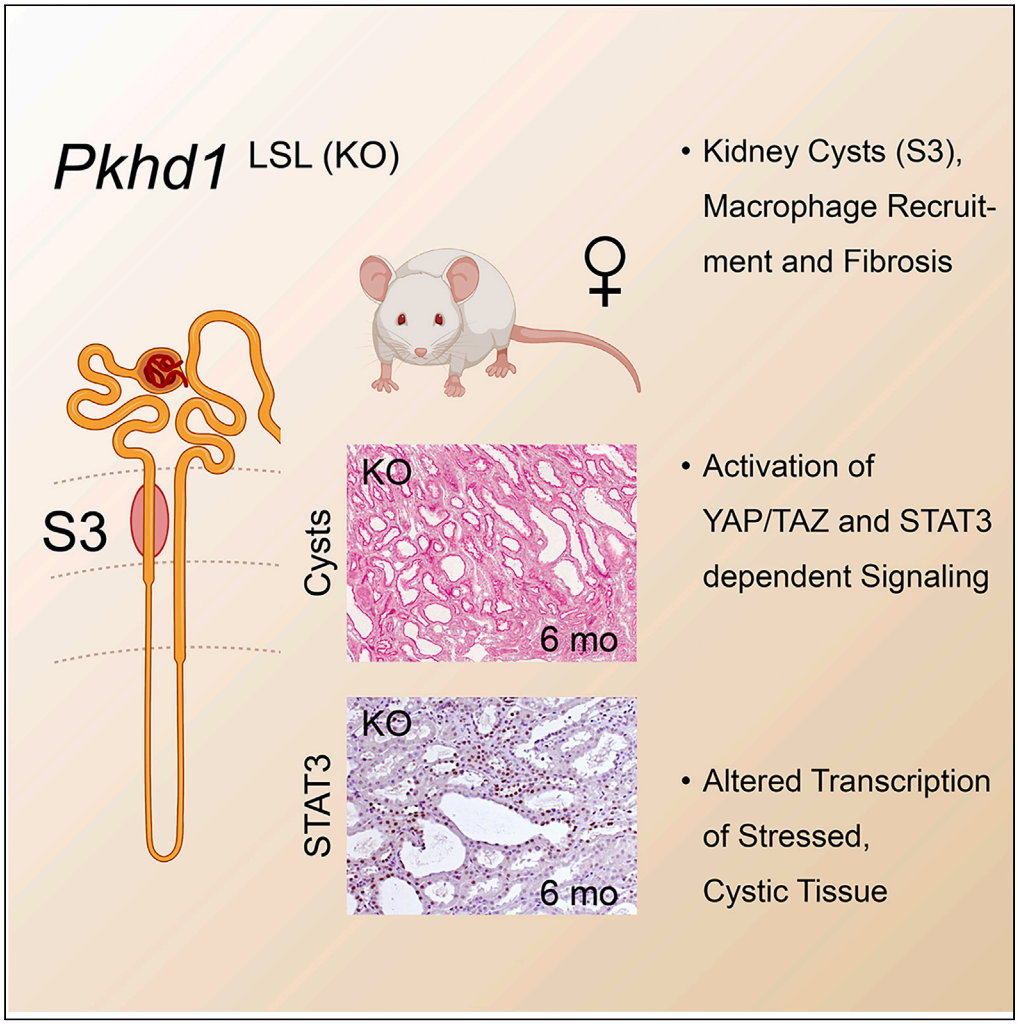

Julia C. Fox, Susanne T. Hahnenstein, Fatima Hassan, Andrea Grund, Dieter Haffner, Wolfgang H. Ziegler

ziegler.wolfgang@mh-hannover.de

Highlights

Late-onset, quantitative kidney cyst phenotype in female *Pkhd1*-knockout mice

Cystogenesis of S3 segments involves cell proliferation, inflammation, and fibrosis

Y705-phosphorylated, nuclear STAT3 is strongly enhanced in cyst-lining epithelia

Increased STAT3-dependent transcription in cystic kidney tissue of *Pkhd1* knockout

Fox et al., iScience *27*, 109487
April 19, 2024
https://doi.org/10.1016/j.isci.2024.109487

iScience

CellPress
OPEN ACCESS

Article

Defects of renal tubular homeostasis and cystogenesis in the *Pkhd1* knockout

Julia C. Fox,[1] Susanne T. Hahnenstein,[1] Fatima Hassan,[1] Andrea Grund,[1] Dieter Haffner,[1] and Wolfgang H. Ziegler[1,2,*]

SUMMARY

Loss of *PKHD1*-gene function causes autosomal recessive polycystic kidney disease (ARPKD) characterized by bilateral severely enlarged kidneys and congenital liver fibrosis requiring kidney replacement therapy most frequently during childhood. Studies using renal tissue from ARPKD patients suggest cyst promotion by suppressed hippo activity and enhanced Src/STAT3-signaling. We address renal homeostasis in female *Pkhd1*-knockout mice, aged 3 to 9 months, and observe features in common with late-onset ARPKD. *Pkhd1*-knockout animals show significant increase in kidney and liver weight with preserved organ function. Kidney cyst formation of the S3 segment is accompanied by macrophage recruitment and fibrotic remodeling. Cystic epithelia display increased proliferation, high levels of nuclear YAP/TAZ, and enhanced apoptosis. Y705-phosphorylated STAT3 is strongly enhanced in nuclei of cyst-lining epithelia. In this *Pkhd1*-deficiency model, stressed cystic epithelia expose the altered signaling pattern and disease-related mechanisms deemed relevant to human ARPKD, and thus may allow identification of therapeutic targets of this disease.

INTRODUCTION

Autosomal recessive polycystic kidney disease (ARPKD) is a rare hereditary disease and belongs to the group of ciliopathies.[1] It affects 1 in 20,000 live births and is one of the most frequent causes for end-stage kidney disease in children and young adults. Children are usually diagnosed *in utero* or at birth. ARPKD is characterized by bilateral polycystic kidneys, congenital liver fibrosis due to ductal plate malformation, and hypoplasia of the lungs.[2–4] Progressive liver fibrosis may result in portal hypertension while liver function is largely preserved in ARPKD patients. The disease is caused by pathogenic variants in the polycystic kidney and hepatic disease gene 1 (*PKHD1*) which encodes the protein fibrocystin/polyductin (FPC). Biallelic *PKHD1* mutation leads to a loss of FPC function and, dependent on severity, affects embryonal development and/or homeostasis of epithelial tissue. The variable phenotype of affected patients depends on the type of mutation of both alleles, on the age of disease manifestation, and genetic background. Two truncating *PKHD1* mutations are associated with a more severe phenotype. Due to the broad distribution and low frequency of private pathogenic variants, further phenotype-to-genotype relations are difficult to establish.[5–7]

Apart from kidney replacement therapies, dialysis and transplantation, and liver transplantation, there is no curative treatment strategy available, and patients are treated only symptomatically. To date, development of new pharmacological interventions is mostly restricted to advances in treatment of the more frequent autosomal dominant polycystic kidney disease (ADPKD).[3,8–10] This can be rationalized based on a considerable overlap in molecular aspects of known disease mechanisms and is also supported by the phenotypic outcome of mouse models combining both PKD genetics.[11]

The protein FPC is a type 1 transmembrane protein of 4,074 amino acids, which localizes to the primary cilia, and furthermore, to the basal body and other cellular compartments in kidney epithelium, bile ducts, and epithelia of lung and pancreas.[12–15] The short cytoplasmatic protein domain of FPC is a target of Notch-like processing and can translocate to the nucleus.[16] Further (or alternative) processing can lead to targeting of cytoplasmic FPC domain protein to mitochondria and affect their function.[17] Besides a proposed involvement of FPC in signal transduction of cilia, due to its ciliary targeting sequence,[18] the protein was also associated with the control of epithelial morphogenesis, affecting mechanics of cell-cell and cell-extracellular matrix adhesion of epithelial cells[19,20] and regulation of RhoA activity via the E3 family of ligases.[21]

While the function of FPC protein, based on molecular interactions, remains insufficiently understood, different signaling pathways, including cAMP and mammalian target of rapamycin (mTOR), have been linked to the development and progression of ARPKD.[22–24] In addition, altered hippo signaling is expected to play a central role in PKD. This pathway regulates organ size and proliferation by restricting activity of two transcriptional co-regulators, Yes-associated protein 1 (YAP) and WW domain-containing transcription regulator 1 (TAZ). Nuclear localization of YAP/TAZ is frequently detected in cystic renal tissue,[25–27] and epithelial YAP activation was shown in ARPKD patients.[28,29] More

[1]Department of Pediatric Kidney, Liver and Metabolic Diseases, Hannover Medical School, Hannover, Germany
[2]Lead contact
*Correspondence: ziegler.wolfgang@mh-hannover.de
https://doi.org/10.1016/j.isci.2024.109487

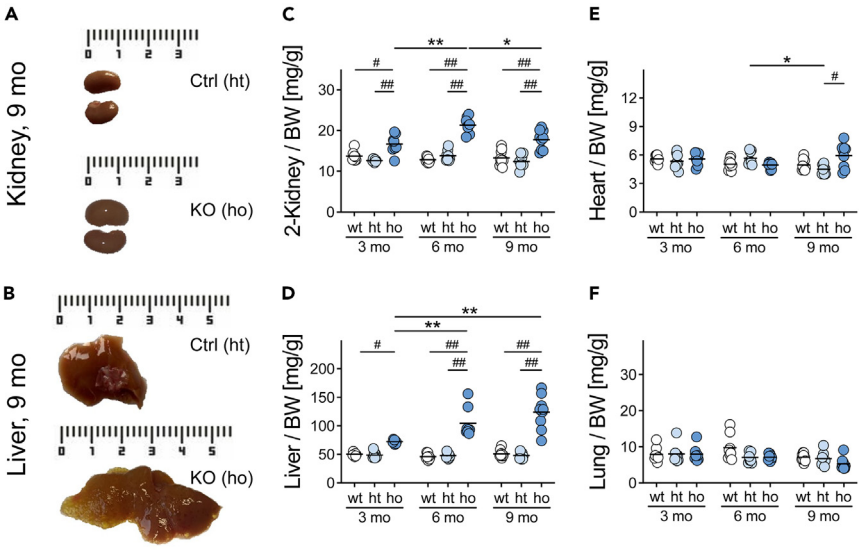

Figure 1. Control of organ size in *Pkhd1* knockout

Large organ size of the kidneys (A) and the liver (B) is displayed by representative organs of knockout (ho) and control (ht) animals aged 9 months (mo). Profiles of the relative organ weight, as compared to the total body weight (BW), indicate enhanced 2-kidney weight (C), peaking at 6 months of age, and continuous growth of massively enlarged liver weight (D) of *Pkhd1*-knockout animals, as compared to both control groups. In old knockout animals, hearts (E) appear to become bigger by trend and lungs (F) smaller. (n = 8–9 animals, and means/group, time point). Statistics: two-way ANOVA, Tukey's; comparisons marked by (*) relate to the same genetic group at different age and by (#) to age-matched groups, indicating $p \leq 0.05$ and $p \leq 0.001$ by */# and **/##. Ruler (cm).

recently, the cytoplasmic protein domain of FPC was proposed to modulate phosphorylation and activity of the signal transducer and activator of transcription 3 (STAT3) via inhibition of the non-receptor tyrosine kinase Src; activation of both was observed in cystic renal epithelia of ARPKD patients[30]

Here, consequences of the *Pkhd1* knockout were studied in BALB/cJ mice carrying a targeted mutation of the *Pkhd1* gene.[31] Previous analyses of this model in a mixed-strain background had established cystic liver disease observed in all animals of both sexes and a mild, inconsistent cyst development observed in kidneys of females only.[31] Despite multiple approaches and reports of different genetic models,[32] to date, there is no suitable genetic mouse model of ARPKD available that can be employed to analyze the tissue defects and the progress of cystic kidney disease in absence of FPC protein expression. Thus, we re-evaluated the mouse model introduced by the Christopher Ward laboratory[31] with the aim to establish a model for late-onset cystic kidney disease originating from ARPKD genetics. This *Pkhd1*-deficiency model of PKD highlights the functional involvement of FPC protein in preserving tissue homeostasis.

RESULTS

Our analysis of the *Pkhd1* knockout[31] was based on female BALB/cJ animals, at the age of 3, 6, and 9 months, comparing the group of homozygous (ho), *Pkhd1* (tm/tm) mice lacking FPC expression, to the control groups of heterozygous (ht) *Pkhd1* (wt/tm) and wild-type (wt) *Pkhd1* (wt/wt) animals. Both control groups behaved identical throughout the entire study and did not develop any sign of cystic disease.

Pkhd1-knockout mice develop large kidneys and massively increased livers

Figure 1 shows the trends of relative organ weight for kidneys, liver, heart, and lung, at the indicated animal age. In the *Pkhd1* knockout, the kidney weight (Figure 1C) was consistently enhanced in all animals and significantly larger at all time points. Starting with about one-third (27%) at the age of 3 months, the gain of relative weight peaked at 6 months (60%) and was somewhat reduced at 9 months (42%) as compared to controls. The observed, massive and continuous growth of the liver in knockout animals (Figure 1D) is consistent with regeneration of tissue to replace highly cystic liver lobes; incidence of the latter was readily detected during dissection. At the age of 9 months, the relative liver weight was increased by 2.5-fold with absolute values of up to 4 g of liver observed in *Pkhd1*-knockout animals. The two control groups of heterozygous and wild-type mice revealed no differences in their absolute and relative kidney and liver weights throughout all time points (Figures 1C and 1D). Furthermore, heart, lung and pancreas (not shown) were weighted. Both the absolute and relative organ weights showed some trends but no consistent differences of the *Pkhd1* knockout to both control genotypes, for any of the organs listed (Figures 1E and 1F).

Kidney and liver function are preserved in the *Pkhd1* knockout

Next, blood and urine samples of the *Pkhd1*knockout, heterozygous and wild-type animals were analyzed (Table 1; wild-type indistinguishable from heterozygous animals, not shown). Although both kidney and liver were significantly enlarged in the knockout, kidney parameters in

Table 1. Weight distributions, and parameters of kidney and liver function in animal cohorts

		Ctrl (ht)			KO (ho)		
Parameter	Unit	3 months	6 months	9 months	3 months	6 months	9 months
Body weight	g	22.6 ± 1.6	23.5 ± 1.5	28.0 ± 4.4	21.3 ± 1.9	# 25.1 ± 2.0	29.5 ± 2.9
2-Kidney weight	g	0.31 ± 0.02	0.32 ± 0.04	0.34 ± 0.03	# 0.35 ± 0.04	## 0.53 ± 0.06	## 0.53 ± 0.05
Liver weight	g	1.14 ± 0.12	1.13 ± 0.14	1.13 ± 0.12	1.54 ± 0.16	## 2.65 ± 0.78	## 3.62 ± 0.77
BUN[a]	mg/dL	42.2 ± 5.1	40.2 ± 10.1	42.8 ± 7.3	46.0 ± 11.2	46.0 ± 4.4	45.2 ± 5.4
Serum creatinine	mg/dL	0.1 ± 0.6	0.4 ± 0.6	0.4 ± 0.7	0.3 ± 0.5	0.1 ± 0.3	0.7 ± 0.8
Serum albumin	mg/dL	34.4 ± 1.4	33.8 ± 2.2	35.5 ± 2.4	33.4 ± 2.4	31.6 ± 2.7	# 30.1 ± 4.2
Urine albumin	mg/dL	4.6 ± 9.6	10.4 ± 8.4	13.2 ± 8.3	9.6 ± 6.4	8.1 ± 5.0	17.1 ± 18.2
AST[b]	UI/L	95.7 ± 35.7	96.6 ± 32.7	112.2 ± 38.1	105.7 ± 40.0	125.3 ± 48.9	142.6 ± 95.6
ALT[c]	UI/L	46.2 ± 12.8	52.8 ± 10.2	60.6 ± 17.3	62.3 ± 27.5	73.9 ± 32.9	89.4 ± 82.8
Uric acid	mg/dL	1.64 ± 0.44	1.59 ± 0.69	1.28 ± 0.37	1.49 ± 0.26	1,35 ± 0.52	1.97 ± 0.85
Total bilirubin	mg/dL	0.55 ± 0.10	0.07 ± 0.05	0.11 ± 0.03	0.05 ± 0.05	0.11 ± 0.07	0.12 ± 0.09

Parameters were determined in control (Ctrl), *Pkhd1* (wt/tm), and knockout (KO), *Pkhd1* (tm/tm), mice at 3 to 9 months of age (n = 6–9). Values are given as mean ± SD. Statistics: Two-way ANOVA, Tukey's; Comparisons marked by (#) relate to age-matched groups, indicating $p \leq 0.05/0.001$ by #/##.

[a]blood urea nitrogen (BUN).

[b]aspartate transaminase (AST).

[c]alanine transaminase (ALT).

urine and blood samples indicated no significant change of kidney function. Blood urea nitrogen, serum creatinine, or uric acid were not elevated at any time point in the samples of *Pkhd1*-knockout animals, nor in animals of the control groups. Preserved kidney function of knockout animals reflects a slowly progressive disease development. Furthermore, analysis of liver parameters revealed the trend toward reduced synthesis capacity, as indicated by lower levels of the serum albumin in knockout animals aged 9 months, compared to controls. Other parameters such as transaminases and bilirubin provided no further indication of restricted liver function (Table 1).

Kidney cysts originate from proximal tubule

In ARPKD patients, cystic dilations in the kidney mainly originate from distal tubules and collecting ducts. In this *Pkhd1*-knockout mouse model, cysts emerge from the S3 segment of proximal tubules (Figures 2A and 2B). Origin of cysts is first indicated by a positive stain of cystic epithelia for aquaporin-1, a marker of the proximal tubule. Second, cysts are located at the corticomedullary border and coincide with a pronounced periodic acid-Schiff (PAS) stain of the glycocalyx, characteristic for brush border membranes of the proximal tubules. Third, cyst-lining epithelial cells exhibit no positive staining for other epithelial markers, the collecting duct marker aquaporin-2 and the distal tubule marker uromodulin, respectively. Occasional staining of individual cyst-lining cells by the collecting duct marker Dolichos biflorus agglutinin (Figure S1A) may be related to a loss of epithelial cell differentiation in cystic epithelia. A previous study in PCK rats, an orthologous rat model of ARPKD, showed increased renal expression of the amiloride-sensitive sodium channel ENaC in cysts of the collecting duct.[21] In *Pkhd1*-knockout mice, ENaC was detected in cyst-lining epithelia at all time points, indicating atypical expression of the channel in dilated S3 segments (Figure S1B).

Growth of kidney cysts is limited by the accompanying progressive fibrosis

To follow the time course of cyst formation in *Pkhd1* knockout, the cystic index (Figure 2C) was determined as ratio of cumulative cyst area to whole cortex area (Figure S1C). Further parameters extracted from entire cross sections, stained by hematoxylin PAS, were the number of cysts (Figure 2D) and the average size of cysts (not shown). All quantitative cyst parameters report an initial cyst growth in the *Pkhd1*-knockout mice, up to 6 months, followed by a decrease. At the age of 3 months, kidney cyst formation is initiated (Figure 2C). While cysts are not (yet) consistently observed in all of the knockout animals, the dilated cystic areas (cystic index, number) are already increased by 6-fold on average, relative to control groups. Between 3 and 6 months of age, both the number of cysts and the cystic index increase by 4- to 5-fold in the *Pkhd1*knockouts, claiming 8% of the whole cortex area and, thereafter, decline to half of the value in 9-month-old animals (Figures 2C and 2D). Development of proximal tubule cysts is limited to *Pkhd1*-knockout mice, whereas no renal cysts were observed in heterozygous and wild-type control animals.

To address fibrotic remodeling during disease progression (Figures 2E and 2F), Sirius Red (SR) staining was performed. The fibrotic index represents the area of collagen fibers per kidney cross section in relation to the whole cortex area (Figure S1D). Dense collagen fibers and fibrotic regions (Figure 2E) are detectable at 6 months and further increased at 9 months of age in the *Pkhd1*-knockout mice. The collagen fibers, while spreading throughout the entire cortex area, are particularly enriched around cystic lesions at the corticomedullary border. Compared to controls, the fibrotic index (Figure 2F) increases by 10- and 15-fold in 6- and 9-month-old *Pkhd1*-knockout animals, respectively, covering up to 3% of the cortex area. Enhanced TGF-β signaling related to renal fibrosis[33,34] is confirmed by increased expression of Smad 3 target genes *Ctgf*, *Col1a2*, and *Tgf-β1* itself, in tissue extracts (Figures S1E–S1G).

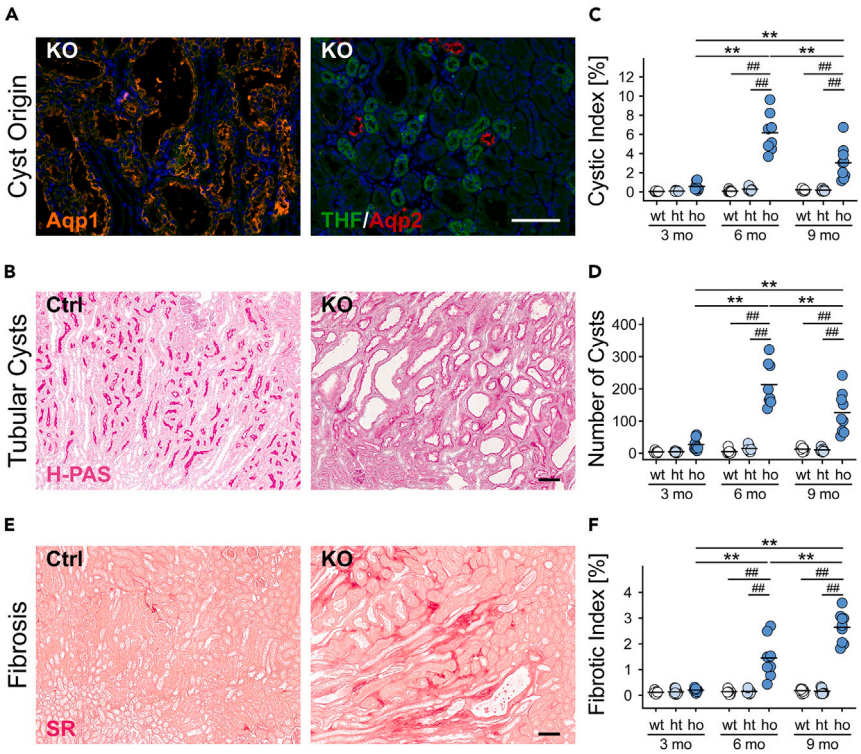

Figure 2. Origin and growth of kidney cysts, and associated fibrosis in *Pkhd1* knockout

(A) Cystic epithelia are positive for the proximal tubule marker aquaporin-1 (Aqp1) and staining of the brush borders (PAS), with no overlap for markers of the distal tubule, uromodulin/Tamm-Horsfall protein (THF), and of the collecting duct epithelia, aquaporin-2 (Aqp2), respectively.

(B) Representative images show tissue sections of 6-month-old heterozygous control (Ctrl) and knockout (KO) animals. Extraction of the cystic index (C) and the number of cysts (D) from entire, hematoxylin periodic acid-Schiff (H-PAS)-stained cross sections of the kidney (see also Figure S1C) indicate a strong and consistent increase of cysts in *Pkhd1* knockout (ho). Cyst growth is limited by a continuous increase of the fibrotic areas, as revealed by Sirius Red (SR) staining of the collagen matrix (E) and the fibrotic index (F). There is neither indication of cyst formation nor of fibrotic lesions in kidney sections of heterozygous (ht) and wild-type (wt) controls; see also Figures S1A–S1G. (n = 8–9 animals, and means/group, time point). Statistics: two-way ANOVA, Tukey's; comparisons marked by (*) relate to the same genetic group at different age and by (#) to age-matched groups, indicating $p \leq 0.05$ and $p \leq 0.001$ by */# and **/##. Size bars: 100 μm.

Cyst growth is associated with recruitment of inflammatory cells in the *Pkhd1* knockout

Sites of inflammation were highlighted using F-4/80 immunostaining to assess the distribution and the enrichment of macrophages (Figure 3A). To quantify the inflammatory process, occurrence of macrophages as stained by F-4/80 was related to the total renal cortex area (Figure 3B). During early cyst development (3 months), there is no evidence for enhanced recruitment of macrophages, and kidney sections of the *Pkhd1*-knockout and the control animals, mostly showing scattered cells, cannot be distinguished. By 6 months, macrophages accumulate in renal tissue of the *Pkhd1* knockout. The F-4/80-positive area is significantly increased and macrophages appear enriched and clustered at the cortex especially around and in-between cysts (Figures 3A and 3B). While macrophage recruitment to cystic epithelia is still enhanced in 9-month-old *Pkhd1*-knockout mice, differences to heterozygous and wild-type tissue decrease with some local enrichment also seen in control animals (Figure 3B). In controls, F-4/80-positive areas remain moderate in size at all time points, showing no significant differences between tissues of both groups. To address distribution of M1 and M2 macrophages, CD68 (macrosialin) co-staining was performed. The ratio of CD68 and F4/80 double-positive M1 macrophages to all F4/80-positive cells is comparably high in *Pkhd1*-knockout tissue at 3 months, and lower than controls, at 6 months of age, when clusters of macrophages surround cystic areas. This observation suggests a prevalence of M2 characteristics in macrophages at sites of inflammation, in 6-month-old *Pkhd1*-knockout mice (Figures S2A and S2B), and mimics reports in mouse models orthologous to ADPKD,[35] where alternatively activated macrophages (M2) were shown to promote tubular cell proliferation.[36]

Pkhd1-knockout tissue exhibits signs of enhanced proliferation and apoptosis

Although a controversy exists whether or not ARPKD is a strongly proliferative disease, a hallmark of disease development is the expansion of the epithelial compartment, due to altered control of cell proliferation. Proliferative activity in the kidney was addressed comparing nuclear Ki67 signals to the total amount of nuclei per section (Figures 3C and 3D). In tissue of 3-month-old *Pkhd1*-knockout mice, the number of proliferative nuclei is already above controls (ht/wt). The frequency of Ki67-positive nuclei peaks in the 6-month-old *Pkhd1*-knockout mice,

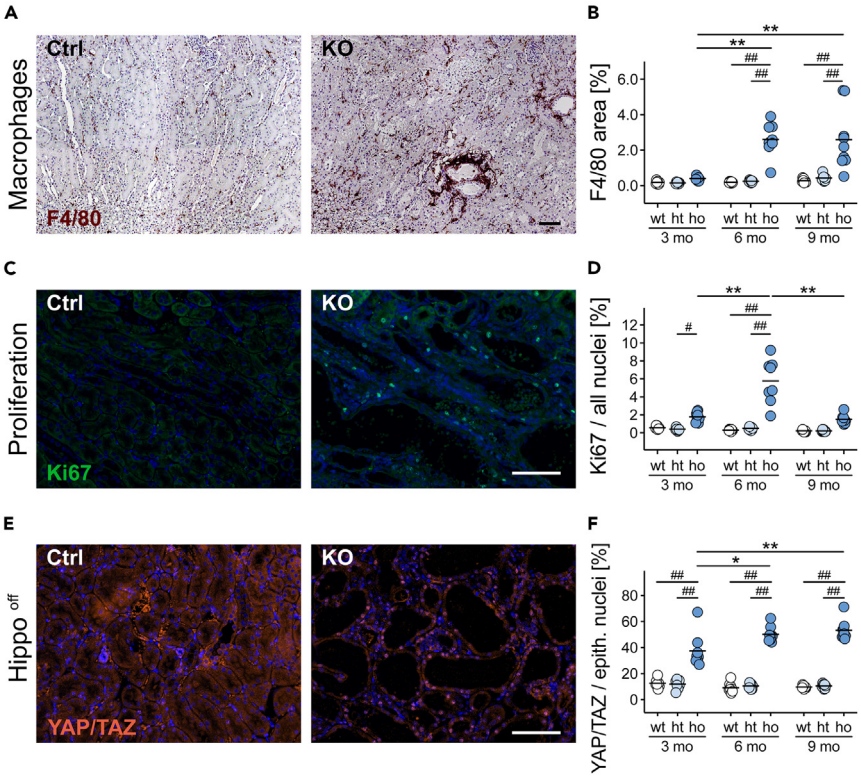

Figure 3. Cyst epithelia attract macrophages and show signs of enhanced proliferation

(A) Distribution of macrophages, as marked by F4/80, reveals their enrichment at cystic lesions of *Pkhd1*-knockout (KO) mice, in contrast to a scattered distribution of resident macrophages in heterozygous (Ctrl) animals, both at the age of 6 months.

(B) The ratio of the F4/80 relative to the cortex area is strongly enhanced in *Pkhd1*-knockout mice (ho) aged 6 and 9 months, and highlights the inflammatory process. Ki67 staining (C, D) indicates the nuclei of proliferating cells and reports enhanced cell proliferation in the kidneys of 6-month-old *Pkhd1*-knockout animals.

(E and F) Nuclear localization of YAP/TAZ indicates inactivation of the hippo pathway (hippo off) in cyst-lining epithelial cells of *Pkhd1*-knockout mice aged 3, 6, and 9 months. Hippo signaling contributes to the control of organ size and homeostasis, and the proliferation of epithelial cells;[27] see also Figures S2A–S2G. (n = 8–9 animals, and means/group, time point). Statistics: two-way ANOVA, Tukey's; comparisons marked by (*) relate to the same genetic group at different age and by (#) to age-matched groups, indicating $p \leq 0.05$ and $p \leq 0.001$ by */# and **/##. Size bars: 100 μm.

reaching 6% of proliferating cells per cross section, and 14-fold of the activity observed on average in the heterozygous and wild-type control animals. In 9-month-old animals, the overall proliferative activity is decreasing by trend in all genotypes and stays moderately enhanced in the *Pkhd1*-knockout mice. The incidence of Ki67-positive nuclei in heterozygous and wild-type animal tissue does not differ significantly between both control groups at any age. Analysis of the proliferating cell nuclear antigen (PCNA), another proliferation marker, in *Pkhd1*-knockout and heterozygous control mice generated comparable results with regards to the incidence of proliferating cells and differences observed between genotypes (Figures S2C and S2D).

Remodeling of diseased kidney epithelia is associated with enhanced apoptosis,[37] which can be studied by cleaved caspase-3 (Casp3) staining. In *Pkhd1*-knockout tissue, we observed cell detritus and dead cells that were shed into cystic lumina and formed clusters (Figures S2E and S2F). The number of Casp3-positive lumina was set in relation to all cystic lumina detected per cross section. While there was only one heterozygous control animal (6 months) that exhibited one Casp3-positive cyst, about one-quarter of all cysts observed in *Pkhd1*-knockout mice, aged 6 or 9 months, contained Casp3-positive material (Figure S2F). These results were reproduced by performing the TUNEL assay in 6-month-old mice. Incidence of TUNEL-positive material was similar to Casp3 staining in cystic dilations of *Pkhd1*-knockout kidneys, and no cell clusters were detected in tissue of controls (Figure S2G).

Cyst formation is accompanied by enhanced nuclear translocation of YAP and TAZ

YAP and TAZ are downstream effectors of the hippo pathway regulating organ size and homeostasis. Nuclear translocation of YAP/TAZ can be triggered by different factors such as energy supply, fibrosis, and mechanical stress.[38] To address a potential inactivation of hippo signaling in the cyst-lining epithelia (Figures 3E and 3F), only epithelial cells were evaluated, counting the YAP/TAZ-positive nuclei relative to total number of epithelial nuclei per tubule. In *Pkhd1* knockout, the incidence of 38%–53% YAP/TAZ-positive nuclei, at all time points, indicates consistently high activation of YAP/TAZ-dependent transcription in the kidney, while levels of 9%–13% as seen in control tissues are

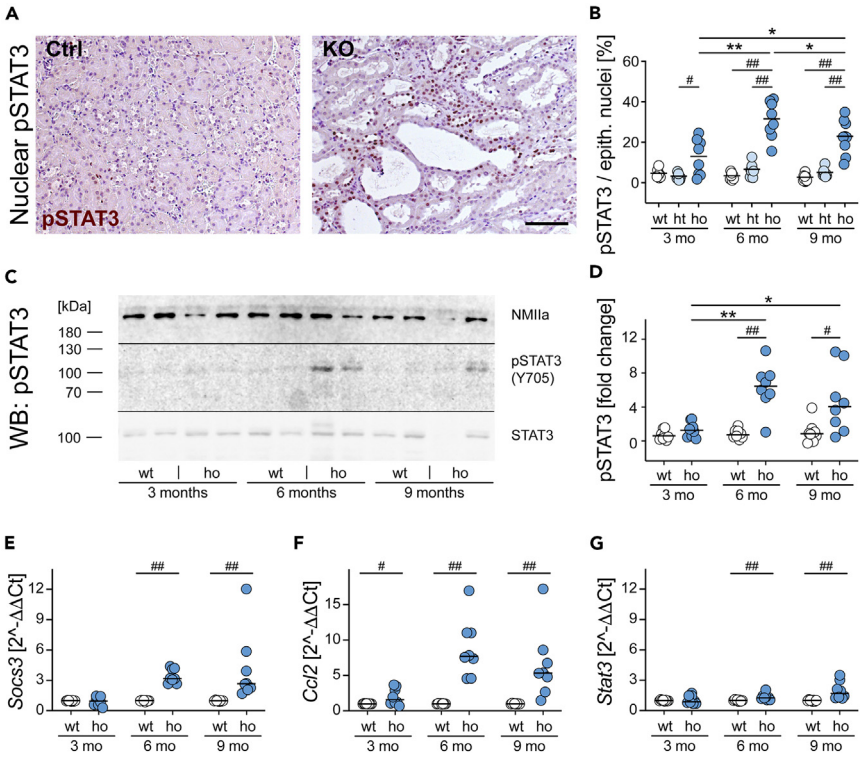

Figure 4. Induction and nuclear localization of pSTAT3 in *Pkhd1*-knockout epithelia

(A) Cyst-lining epithelia in *Pkhd1*-knockout (KO) kidney sections are rich in pSTAT3 (Y705)-stained nuclei, as shown for 6-month-old knockout and control.

(B) STAT3 induction is verified by the ratio of pSTAT3-positive epithelial nuclei detected in the *Pkhd1*-knockout (ho) relative to control mice (wt, ht).

(C and D) Analysis of phosphorylated STAT3 protein levels in kidney extracts using western blot (WB) confirms the activation of STAT3, which is accompanied by enhanced transcription of STAT3 target genes, *Socs3* (E), *Ccl2* (F), and *Stat3* (G) (n = 8–9 animals, and means (B, D) or median (E–G)/group, time point). Statistics: two-way ANOVA, Tukey's (B, D) and Mann-Whitney (E–G); comparisons marked by (*) relate to the same genetic group at different age and by (#) to age-matched groups, indicating $p \leq 0.05$ and $p \leq 0.001$ by */# and **/##. Size bar: 100 μm.

low (Figure 3F). Thus, *Pkhd1*-knockout epithelia show a 3- to 5-fold increase in nuclear YAP/TAZ, which is highest in 6- and 9-month-old mice. As expected for proliferative cystic tissue,[26,39] *c-Myc* expression is elevated in tissue extracts of *Pkhd1*-knockout animals compared to controls with highest levels observed in 3-month-old animals (Figure S2G).

STAT3 signaling is induced in cyst-lining epithelia

Enhanced STAT3 signaling is detected in cystic kidney disease of different genetic origin, and furthermore, the intracellular domain of the protein FPC was reported to negatively modulate Src-dependent phosphorylation and nuclear localization of STAT3. Accordingly, tyrosine Y705-phosphorylated, nuclear STAT3 was observed in cyst-lining epithelia of ARPKD patients.[30] In the *Pkhd1* knockout, the number of pSTAT3 (Y705)-positive nuclei was determined relative to the total number of epithelial nuclei per tubule (Figures 4A and 4B). At 3 months of age, the incidence of nuclear pSTAT3 is moderately increased by 3-fold in kidney epithelia of the *Pkhd1*-knockout mice as compared to controls (wt, ht). Nuclear signals (31%) are 6- to 7-fold increased in 6-month-old animals and level out at the age of 9 months, with 22% of pSTAT3-positive nuclei in the *Pkhd1*-knockout mice. Again, there is no statistically confirmed difference between control groups, albeit a moderate rise is present in the heterozygous mice aged 6 months (Figure 4B). To confirm STAT3 activation on the protein level, kidney extracts of *Pkhd1*-knockout and wild-type controls were studied (Figures 4C and 4D) showing a 6-fold increase in pSTAT3 (Y705) of 6-month-old animals, which highlights enhanced STAT3 signaling in cystic epithelia of *Pkhd1*-knockout mice. Increased expression of STAT3 target genes,[40,41] *Socs3*, *Ccl2*, and *Stat3*, was observed in renal tissue of 6- and 9-month-old *Pkhd1*-knockout mice (Figures 4E–4G).

DISCUSSION

Our study of an ARPKD mouse model, introduced by Bakeberg and colleagues,[31] addresses the evolution and molecular signature of cystic kidney disease, as observed in female *Pkhd1*-knockout animals with a defined BALB/cJ background. The kidney phenotype shows several features in common with a slowly developing, late-onset ARPKD and involves cyst formation of S3 tubular segments, which is accompanied by recruitment of macrophages and continuous fibrotic remodeling. Defective homeostasis and malfunction of tubular epithelia are detected in response to stress factors that are predicted to require FPC protein function. Disease progression is characterized by persistent activation of

YAP/TAZ as well as enhanced STAT3 signaling which was attributed to absence of the FPC intracellular domain. In this model of PKD, we study the relevance of FPC deficiency for the observed defective homeostasis of stressed renal epithelia.

State of cystic epithelia and epithelial cells

Similar to other murine ARPKD models,[32] cyst formation of the kidneys is moderate. Relative organ size of the kidney peaks at 6 months of age and coincides with moderately enhanced cell proliferation, as determined by Ki67 and PCNA staining of nuclei, and with shedding of apoptotic epithelial cells detected in 20%–40% of cyst lumina. Although cyst formation requires expansion of renal tubular epithelia, in this study, there was no time point showing really high proliferative activity. This is in agreement with observations in different epithelial cell models of murine, canine, and human origin which lack FPC protein function. Analysis of cell properties in 2D and 3D culture reveals altered cell-cell interaction and a range from moderately enhanced to reduced cell proliferation that is accompanied by increased apoptotic signaling.[20,37,42,43] In addition, preparations of primary urine-derived renal epithelial cells from ARPKD patients did not provide evidence for a proliferative advantage as compared to cells from healthy donors.[43] In FPC-deficient epithelia, in a way similar to ADPKD, dysregulation of mTOR, B cell lymphoma 2, and caspase pathways was suggested to affect the balance between autophagy and apoptosis, and to thus promote cyst formation.[44] Altered cell-cell interaction of ARPKD epithelia, together with dysregulated proliferation and apoptosis of renal tubular epithelial cells, is expected to alter cellular response to environmental stimuli, modify homeostasis signaling, and thus prime formation of epithelial cysts.

In this model, cystic epithelia show signs of aberrant cell differentiation. In particular, consistently enhanced, atypical expression of the sodium channel ENaC was observed in dilated S3 segments. A study based on the rat ARPKD model reported elevated expression and channel activity of ENaC and proposed that enhanced sodium reabsorption of collecting duct epithelia would contribute to the hypertension observed in PCK rats.[21] Other studies also using PCK rats observed exacerbated cystogenesis, when ENaC expression and activity were inhibited or strongly reduced by a salt-deficient diet.[45,46] Thus, altered expression of ENaC is expected to affect ion transport of *Pkhd1*-deficient, cystic epithelia; however, consequences on disease progression remain to be established.

Origin and localization of epithelial defects

In this late-onset, murine ARPKD model, formation of kidney cyst is moderate and limited to the S3 tubular segment of female mice. In ARPKD patients, formation of fusiform cysts is mostly restricted to collecting ducts, showing highly variable onset and extent of disease progression. This is most likely attributed to differences in penetrance and severity of pathogenic variants of the *Pkhd1* gene, and there is no simple correlation between genotype, onset and phenotypic outcome of PKD in patients.[3,6,7] A study in human tissue documented a transient phase of proximal tube cysts formed during embryonal development. These cysts entirely give way to cysts of the collecting duct in late embryonal stages.[47] Thus, susceptibility of FPC-deficient tubular epithelia to cyst formation can vary with developmental stage and between species. In this context, mice appear to be better protected and develop no early or severe kidney phenotype. Comparison of different murine ARPKD models confirms sensitivity of the proximal tube for cyst formation and shows variability in outcome and penetrance of epithelial defects dependent on the mouse strain.[32,48] There are reports that in addition to proximal tube cysts, murine *Pkhd1* knockout models can show cyst formation of collecting duct epithelia and also affect male animals. A mouse homozygous for the replacement of *Pkhd1* exons 1–3 with a lacZ reporter gene developed progressive renal cystic disease involving proximal tubules, collecting ducts, and glomeruli,[49] and a mouse homozygous for a deletion of *Pkhd1* exons 3 and 4 in a mixed genetic background developed cysts in the collecting ducts and thick ascending limbs.[50] In both cases, kidney cyst formation occurred in both sexes with variable penetrance, and (stress) factors leading to enhanced epithelial susceptibility of these models remain elusive. Although there are no follow-up reports to both models, they have the potential to provide additional information on disease-related mechanisms. In contrast to the mixed strain background used for the initial description of the *Pkhd1* knockout in this study,[31] we observe complete penetrance of kidney defects in all BALB/cJ female mice aged 3 months or older, which is apparent in any tissue section.

Inactivation of the *Pkhd1* gene, as determined also in a different genetic approach, leads to consistent renal cyst formation of female mice only.[31,48] Sex differences become more relevant to the understanding of organ physiology and differential properties relate to tissue function, impact of gene variants, and response to drug treatment. Two observations may help explain both selective occurrence and site of tubular defects in female mice. First, single-cell profiling of mouse kidney revealed prominent differences in expression profiles between the sexes for proximal nephron segments. Highest disparity was detected for gene activity of the S3 segment, highlighting differences in small molecules, lipid, and organic acid metabolism.[51] Second, transport activities of the S3 segment require high glycolytic activity, which makes them sensitive to ischemic acute kidney injury.[52,53] The male S3 segments in mice appear to have better mitochondrial function and higher lysosomal activity, features controlled by androgens, which in male mice may provide a critical capacity to suppress cyst formation in metabolically stressed tissue.[48,54,55] Signs of diminished lysosomal and mitochondrial function were also detected in ARPKD patients,[56–58] and recently, FPC protein function was linked to mitochondrial performance. Protein fragments of the FPC cytoplasmic domain were shown to localize in mitochondria, where they can modify mitochondrial morphology and signal to suppress renal cystogenesis.[17]

Pathogenesis of disease progression

In ARPKD, aberrant activity of the hippo pathway and increased proliferation are expected to promote cystic kidney disease, as known also for other PKD conditions.[3,27,28] YAP/TAZ, two transcriptional regulators controlled by the hippo pathway and other signals, are central to the integration of physical stimuli and metabolic pathways to control cell behavior, proliferation, and tissue regeneration.[38] In this mouse model,

epithelia of *Pkhd1*-knockout mice show consistently high YAP/TAZ activation as indicated by ≥ 30% YAP/TAZ-positive epithelial cell nuclei at all time point analyzed, an increase by 3- to 5-fold compared to controls. While the factors that initiated enhanced transcriptional activity remain to be elucidated, there are key properties of the cystic tissue that can help explain persistent activation of YAP/TAZ in epithelia of *Pkhd1*-knockout animals. These properties—well documented to induce both transcriptional regulators[38]—are (i) altered cell-cell and cell-extracellular matrix interaction, in particular higher force transmission, of FPC-deficient epithelial cells,[19,20] (ii) increasing mechanical stress induced by fibrotic remodeling of the kidney as observed in the model,[59,60] and (iii) metabolic requirements of the S3 segment as discussed previously in combination with enhanced glycolysis and metabolic reprogramming of PKD epithelia.[61–63] Together, these three factors may lead to a self-reinforcing cycle, whereby fibrosis enhances mechanical stress and stimulates proliferation of epithelial cells and fibroblasts, and fibrotic remodeling,[64] while deteriorating tissue function worsens glycolytic stress, which all together further stimulate YAP/TAZ activity.[38] Recruitment of macrophages associated with fibrotic tissue remodeling and cytokines can further contribute to disease progression.[65]

Functional relevance of the FPC cytoplasmic domain

Multiple pathways including high intracellular cAMP and mechanical stress lead to activation of the non-receptor tyrosine kinase Src, as detected by Y416 phosphorylation, and subsequently, to STAT3-dependent transcription. STAT3 activation is proposed to promote disease progression in PKD and to modulate inflammation.[41,66,67] In cell culture, cAMP-induced Src activation is inhibited by (over)expression of the FPC cytoplasmic protein domain (FPCc) in wild-type HEK293T cells. FPCc causes reduction of Src phosphorylation and STAT3-dependent promoter activity.[30] These results suggest a model, whereby the FPC cytoplasmic domain can interfere with Src activation to limit STAT3-dependent transcription, and FPC may have a protective role in preserving epithelial homeostasis. In ARPKD epithelia which gradually develop a cystic phenotype, (reduction or) absence of FPC protein will permit enhanced STAT3 activation, as these epithelia are continuously stressed by PKD-related signals. Consistently, *Pkhd1*-knockout mice show pronounced nuclear localization of pSTAT3 and a corresponding increase of total Y705-phosphorylated STAT3 in kidney extracts rising in parallel to cytogenesis. In a 3D culture model of cAMP-induced cyst formation by pIMDCK cells,[68] protective effects of FPCc protein expression can be studied. Using several *Pkhd1*-knockout cell lines, we observe that in agreement with the proposed model, controlled expression of FPCc can suppress cyst formation and concomitantly limit Src/STAT3 signaling as detected by a strong reduction in phosphorylated Y416 Src and Y705 STAT3 (Hassan et al., unpublished).

We propose that activation of STAT3 in the late-onset ARPKD mouse model reflects absence of the FPC cytoplasmic domain, and furthermore, promotes cystogenesis. This is in agreement with results in ARPKD patients showing enhanced Src/STAT3 phosphorylation in cyst-lining epithelia, and with the severe phenotypic outcome of two patients with truncating *PKHD1* variants of the cytoplasmic protein domain.[30] In a further mouse model of ARPKD, removal of exon 67, the last exon in FPC which encodes the major part of the cytoplasmic domain, did not result in a detectable liver (or kidney) phenotype of *Pkhd1* Δexon67 mice.[69] However, when combined with a delayed-onset ADPKD model (*Pkd1*$^{v/v}$), cytogenesis of the kidney was strongly enhanced in double-mutant mice.[17] This suggests that function of the FPC cytoplasmic domain becomes critical only, when epithelial homeostasis is challenged by cyst-inducing stress. This protective function of the protein domain may help explain the low penetrance of kidney phenotypes in murine ARPKD models.[32]

In summary, this slowly developing, late-onset model of kidney cystogenesis stresses the relevance of Src inhibition (and related tyrosine kinases) as discussed for clinical use in ADPKD and ARPKD.[10,70,71] In addition, restoration of FPC cytoplasmic domain function in cystic tissue can enhance mitochondrial function and attenuate stress-related Src activity and STAT3-dependent transcription, which together are predicted to protect the function of renal tubular epithelia and their homeostasis. The presented murine model reveals mechanisms triggered by *Pkhd1* deficiency, some of which are also observed in and proposed relevant to human ARPKD. The model is expected to allow the identification of new therapeutic targets and the testing of treatment strategies to prevent progressive organ damage in this severe disease.

Limitations of the study

In this study, analysis of renal cysts was restricted to female *Pkhd1*-knockout animals. While we established a reproducible, quantitative renal cyst phenotype in BALB/cJ mice, this model is not suitable for the analysis of kidney cyst formation in male *Pkhd1*-knockout mice. Ductal plate malformation and congenital liver fibrosis, as part of the ARPKD-related cystic liver disease observed in both sexes, were not addressed in this manuscript.

STAR★METHODS

Detailed methods are provided in the online version of this paper and include the following:

- KEY RESOURCES TABLE
- RESOURCE AVAILABILITY
  - Lead contact
  - Materials availability
  - Data and code availability
- EXPERIMENTAL MODEL AND STUDY PARTICIPANT DETAILS
  - Animals
  - Study approval
- METHOD DETAILS

- Section preparation, immunofluorescence, immunohistochemistry
- Microscopy and quantitative image analysis
- Western Blot
- Quantification of gene expression

- QUANTIFICATION AND STATISTICAL ANALYSIS

SUPPLEMENTAL INFORMATION

Supplemental information can be found online at https://doi.org/10.1016/j.isci.2024.109487.

ACKNOWLEDGMENTS

The authors thank Rachel Gallagher for encouragement to pursue this project and Sebastian Bachmann for his expertise in the interpretation of the kidney damage. J.C.F., S.T.H., and F.H. were supported by the Hannover Biomedical Research School (HBRS). A.G., D.H., and W.H.Z. received support from the German Network for Early Onset Cystic Kidney Disease (NEOCYST) consortium funded by the German Federal Ministry of Education and Research (BMBF) grant 01GM2203H.

AUTHOR CONTRIBUTIONS

W.H.Z. and D.H. - concept of the study; J.C.F., S.T.H., F.H., A.G., D.H., and W.H.Z. - design and validation of experiments; J.C.F., S.T.H., F.H., A.G., and W.H.Z. - acquisition and analysis of data and samples; J.C.F., S.T.H., F.H., A.G., D.H., and W.H.Z. - interpretation of data and clinical parameters; and J.C.F., D.H., and W.H.Z. - draft and/or revision of the manuscript. All authors read, reviewed, and gave their final approval of the work.

DECLARATION OF INTERESTS

The authors declare no competing interests.

Received: July 6, 2023
Revised: January 31, 2024
Accepted: March 8, 2024
Published: March 11, 2024

REFERENCES

1. Hildebrandt, F., Benzing, T., and Katsanis, N. (2011). N. Engl. J. Med. *364*, 1533–1543. https://doi.org/10.1056/NEJMra1010172.
2. Büscher, R., Büscher, A.K., Weber, S., Mohr, J., Hegen, B., Vester, U., and Hoyer, P.F. (2014). Clinical manifestations of autosomal recessive polycystic kidney disease (ARPKD): kidney-related and non-kidney-related phenotypes. Pediatr. Nephrol. *29*, 1915–1925. https://doi.org/10.1007/s00467-013-2634-1.
3. Bergmann, C., Guay-Woodford, L.M., Harris, P.C., Horie, S., Peters, D.J.M., and Torres, V.E. (2018). Polycystic kidney disease. Nat. Rev. Dis. Primers *4*, 50. https://doi.org/10.1038/s41572-018-0047-y.
4. McConnachie, D.J., Stow, J.L., and Mallett, A.J. (2021). Ciliopathies and the Kidney: A Review. Am. J. Kidney Dis. *77*, 410–419. https://doi.org/10.1053/j.ajkd.2020.08.012.
5. Bergmann, C., Senderek, J., Windelen, E., Küpper, F., Middeldorf, I., Schneider, F., Dornia, C., Rudnik-Schöneborn, S., Konrad, M., Schmitt, C.P., et al. (2005). Clinical consequences of PKHD1 mutations in 164 patients with autosomal-recessive polycystic kidney disease (ARPKD). Kidney Int. *67*, 829–848. https://doi.org/10.1111/j.1523-1755.2005.00148.x.
6. Bergmann, C. (2017). Genetics of Autosomal Recessive Polycystic Kidney Disease and Its Differential Diagnoses. Front. Pediatr. *5*, 221. https://doi.org/10.3389/fped.2017.00221.
7. Burgmaier, K., Brinker, L., Erger, F., Beck, B.B., Benz, M.R., Bergmann, C., Boyer, O., Collard, L., Dafinger, C., Fila, M., et al. (2021). Refining genotype-phenotype correlations in 304 patients with autosomal recessive polycystic kidney disease and PKHD1 gene variants. Kidney Int. *100*, 650–659. https://doi.org/10.1016/j.kint.2021.04.019.
8. Guay-Woodford, L.M., Bissler, J.J., Braun, M.C., Bockenhauer, D., Cadnapaphornchai, M.A., Dell, K.M., Kerecuk, L., Liebau, M.C., Alonso-Peclet, M.H., Shneider, B., et al. (2014). Consensus expert recommendations for the diagnosis and management of autosomal recessive polycystic kidney disease: report of an international conference. J. Pediatr. *165*, 611–617. https://doi.org/10.1016/j.jpeds.2014.06.015.
9. Benz, E.G., and Hartung, E.A. (2021). Predictors of progression in autosomal dominant and autosomal recessive polycystic kidney disease. Pediatr. Nephrol. *36*, 2639–2658. https://doi.org/10.1007/s00467-020-04869-w.
10. Liebau, M.C., Hartung, E.A., and Perrone, R.D. (2022). Perspectives on Drug Development in Autosomal Recessive Polycystic Kidney Disease. Clin. J. Am. Soc. Nephrol. *17*, 1551–1554. https://doi.org/10.2215/CJN.04870422.
11. Olson, R.J., Hopp, K., Wells, H., Smith, J.M., Furtado, J., Constans, M.M., Escobar, D.L., Geurts, A.M., Torres, V.E., and Harris, P.C. (2019). Synergistic Genetic Interactions between Pkhd1 and Pkd1 Result in an ARPKD-Like Phenotype in Murine Models. J. Am. Soc. Nephrol. *30*, 2113–2127. https://doi.org/10.1681/ASN.2019020150.
12. Ward, C.J., Yuan, D., Masyuk, T.V., Wang, X., Punyashthiti, R., Whelan, S., Bacallao, R., Torra, R., LaRusso, N.F., Torres, V.E., and Harris, P.C. (2003). Cellular and subcellular localization of the ARPKD protein; fibrocystin is expressed on primary cilia. Hum. Mol. Genet. *12*, 2703–2710. https://doi.org/10.1093/hmg/ddg274.
13. Menezes, L.F.C., Cai, Y., Nagasawa, Y., Silva, A.M.G., Watkins, M.L., Da Silva, A.M., Somlo, S., Guay-Woodford, L.M., Germino, G.G., and Onuchic, L.F. (2004). Polyductin, the PKHD1 gene product, comprises isoforms expressed in plasma membrane, primary cilium, and cytoplasm. Kidney Int. *66*, 1345–1355. https://doi.org/10.1111/j.1523-1755.2004.00844.x.
14. Wang, S., Luo, Y., Wilson, P.D., Witman, G.B., and Zhou, J. (2004). The autosomal recessive polycystic kidney disease protein is localized to primary cilia, with concentration in the basal body area. J. Am. Soc. Nephrol. *15*, 592–602. https://doi.org/10.1097/01.asn.0000113793.12558.1d.
15. Zhang, J., Wu, M., Wang, S., Shah, J.V., Wilson, P.D., and Zhou, J. (2010). Polycystic kidney disease protein fibrocystin localizes to the mitotic spindle and regulates spindle bipolarity. Hum. Mol. Genet. *19*, 3306–3319. https://doi.org/10.1093/hmg/ddq233.

16. Kaimori, J.Y., Nagasawa, Y., Menezes, L.F., Garcia-Gonzalez, M.A., Deng, J., Imai, E., Onuchic, L.F., Guay-Woodford, L.M., and Germino, G.G. (2007). Polyductin undergoes notch-like processing and regulated release from primary cilia. Hum. Mol. Genet. *16*, 942–956. https://doi.org/10.1093/hmg/ddm039.
17. Walker, R.V., Yao, Q., Xu, H., Maranto, A., Swaney, K.F., Ramachandran, S., Li, R., Cassina, L., Polster, B.M., Outeda, P., et al. (2023). Fibrocystin/Polyductin releases a C-terminal fragment that translocates into mitochondria and suppresses cystogenesis. Nat. Commun. *14*, 6513. https://doi.org/10.1038/s41467-023-42196-4.
18. Follit, J.A., Li, L., Vucica, Y., and Pazour, G.J. (2010). The cytoplasmic tail of fibrocystin contains a ciliary targeting sequence. J. Cell Biol. *188*, 21–28. https://doi.org/10.1083/jcb.200910096.
19. Israeli, S., Amsler, K., Zheleznova, N., and Wilson, P.D. (2010). Abnormalities in focal adhesion complex formation, regulation, and function in human autosomal recessive polycystic kidney disease epithelial cells. Am. J. Physiol. Cell Physiol. *298*, C831–C846. https://doi.org/10.1152/ajpcell.00032.2009.
20. Ziegler, W.H., Soetje, B., Marten, L.P., Wiese, J., Burute, M., and Haffner, D. (2020). Fibrocystin Is Essential to Cellular Control of Adhesion and Epithelial Morphogenesis. Int. J. Mol. Sci. *21*, 5140. https://doi.org/10.3390/ijms21145140.
21. Kaimori, J.Y., Lin, C.C., Outeda, P., Garcia-Gonzalez, M.A., Menezes, L.F., Hartung, E.A., Li, A., Wu, G., Fujita, H., Sato, Y., et al. (2017). NEDD4-family E3 ligase dysfunction due to PKHD1/Pkhd1 defects suggests a mechanistic model for ARPKD pathobiology. Sci. Rep. *7*, 7733. https://doi.org/10.1038/s41598-017-08284-4.
22. Wang, X., Gattone, V., 2nd, Harris, P.C., and Torres, V.E. (2005). Effectiveness of vasopressin V2 receptor antagonists OPC-31260 and OPC-41061 on polycystic kidney disease development in the PCK rat. J. Am. Soc. Nephrol. *16*, 846–851. https://doi.org/10.1681/ASN.2004121090.
23. Fischer, D.C., Jacoby, U., Pape, L., Ward, C.J., Kuwertz-Broeking, E., Renken, C., Nizze, H., Querfeld, U., Rudolph, B., Mueller-Wiefel, D.E., et al. (2009). Activation of the AKT/mTOR pathway in autosomal recessive polycystic kidney disease (ARPKD). Nephrol. Dial. Transplant. *24*, 1819–1827. https://doi.org/10.1093/ndt/gfn744.
24. Janssens, P., Weydert, C., De Rechter, S., Wissing, K.M., Liebau, M.C., and Mekahli, D. (2018). Expanding the role of vasopressin antagonism in polycystic kidney diseases: From adults to children? Pediatr. Nephrol. *33*, 395–408. https://doi.org/10.1007/s00467-017-3672-x.
25. Cai, J., Song, X., Wang, W., Watnick, T., Pei, Y., Qian, F., and Pan, D. (2018). A RhoA-YAP-c-Myc signaling axis promotes the development of polycystic kidney disease. Genes Dev. *32*, 781–793. https://doi.org/10.1101/gad.315127.118.
26. Lee, E.J., Seo, E., Kim, J.W., Nam, S.A., Lee, J.Y., Jun, J., Oh, S., Park, M., Jho, E.H., Yoo, K.H., et al. (2020). TAZ/Wnt-beta-catenin/c-MYC axis regulates cystogenesis in polycystic kidney disease. Proc. Natl. Acad. Sci. USA *117*, 29001–29012. https://doi.org/10.1073/pnas.2009334117.
27. Müller, R.U., and Schermer, B. (2020). Hippo signaling-a central player in cystic kidney disease? Pediatr. Nephrol. *35*, 1143–1152. https://doi.org/10.1007/s00467-019-04299-3.
28. Happé, H., van der Wal, A.M., Leonhard, W.N., Kunnen, S.J., Breuning, M.H., de Heer, E., and Peters, D.J.M. (2011). Altered Hippo signalling in polycystic kidney disease. J. Pathol. *224*, 133–142. https://doi.org/10.1002/path.2856.
29. Jiang, L., Sun, L., Edwards, G., Manley, M., Jr., Wallace, D.P., Septer, S., Manohar, C., Pritchard, M.T., and Apte, U. (2017). Increased YAP Activation Is Associated With Hepatic Cyst Epithelial Cell Proliferation in ARPKD/CHF. Gene Expr. *17*, 313–326. https://doi.org/10.3727/105221617X15034976037343.
30. Dafinger, C., Mandel, A.M., Braun, A., Göbel, H., Burgmaier, K., Massella, L., Mastrangelo, A., Dötsch, J., Benzing, T., Weimbs, T., et al. (2020). The carboxy-terminus of the human ARPKD protein fibrocystin can control STAT3 signalling by regulating SRC-activation. J. Cell Mol. Med. *24*, 14633–14638. https://doi.org/10.1111/jcmm.16014.
31. Bakeberg, J.L., Tammachote, R., Woollard, J.R., Hogan, M.C., Tuan, H.F., Li, M., van Deursen, J.M., Wu, Y., Huang, B.Q., Torres, V.E., et al. (2011). Epitope-tagged Pkhd1 tracks the processing, secretion, and localization of fibrocystin. J. Am. Soc. Nephrol. *22*, 2266–2277. https://doi.org/10.1681/ASN.2010111173.
32. Cordido, A., Vizoso-Gonzalez, M., and Garcia-Gonzalez, M.A. (2021). Molecular Pathophysiology of Autosomal Recessive Polycystic Kidney Disease. Int. J. Mol. Sci. *22*, 6523. https://doi.org/10.3390/ijms22126523.
33. Meng, X.M., Nikolic-Paterson, D.J., and Lan, H.Y. (2016). TGF-beta: the master regulator of fibrosis. Nat. Rev. Nephrol. *12*, 325–338. https://doi.org/10.1038/nrneph.2016.48.
34. Sureshbabu, A., Muhsin, S.A., and Choi, M.E. (2016). TGF-beta signaling in the kidney: profibrotic and protective effects. Am. J. Physiol. Renal Physiol. *310*, F596–F606. https://doi.org/10.1152/ajprenal.00365.2015.
35. Karihaloo, A., Koraishy, F., Huen, S.C., Lee, Y., Merrick, D., Caplan, M.J., Somlo, S., and Cantley, L.G. (2011). Macrophages promote cyst growth in polycystic kidney disease. J. Am. Soc. Nephrol. *22*, 1809–1814. https://doi.org/10.1681/ASN.2011010084.
36. Lee, S., Huen, S., Nishio, H., Nishio, S., Lee, H.K., Choi, B.S., Ruhrberg, C., and Cantley, L.G. (2011). Distinct macrophage phenotypes contribute to kidney injury and repair. J. Am. Soc. Nephrol. *22*, 317–326. https://doi.org/10.1681/ASN.2009060615.
37. Hu, B., He, X., Li, A., Qiu, Q., Li, C., Liang, D., Zhao, P., Ma, J., Coffey, R.J., Zhan, Q., and Wu, G. (2011). Cystogenesis in ARPKD results from increased apoptosis in collecting duct epithelial cells of Pkhd1 mutant kidneys. Exp. Cell Res. *317*, 173–187. https://doi.org/10.1016/j.yexcr.2010.09.012.
38. Totaro, A., Panciera, T., and Piccolo, S. (2018). YAP/TAZ upstream signals and downstream responses. Nat. Cell Biol. *20*, 888–899. https://doi.org/10.1038/s41556-018-0142-z.
39. Lakhia, R., Mishra, A., Biggers, L., Malladi, V., Cobo-Stark, P., Hajarnis, S., and Patel, V. (2023). Enhancer and super-enhancer landscape in polycystic kidney disease. Kidney Int. *103*, 87–99. https://doi.org/10.1016/j.kint.2022.08.039.
40. Takakura, A., Nelson, E.A., Haque, N., Humphreys, B.D., Zandi-Nejad, K., Frank, D.A., and Zhou, J. (2011). Pyrimethamine inhibits adult polycystic kidney disease by modulating STAT signaling pathways. Hum. Mol. Genet. *20*, 4143–4154. https://doi.org/10.1093/hmg/ddr338.
41. Talbot, J.J., Song, X., Wang, X., Rinschen, M.M., Doerr, N., LaRiviere, W.B., Schermer, B., Pei, Y.P., Torres, V.E., and Weimbs, T. (2014). The cleaved cytoplasmic tail of polycystin-1 regulates Src-dependent STAT3 activation. J. Am. Soc. Nephrol. *25*, 1737–1748. https://doi.org/10.1681/ASN.2013091026.
42. Mai, W., Chen, D., Ding, T., Kim, I., Park, S., Cho, S.Y., Chu, J.S.F., Liang, D., Wang, N., Wu, D., et al. (2005). Inhibition of Pkhd1 impairs tubulomorphogenesis of cultured IMCD cells. Mol. Biol. Cell *16*, 4398–4409. https://doi.org/10.1091/mbc.e04-11-1019.
43. Ziegler, W.H., Lüdiger, S., Hassan, F., Georgiadis, M.E., Swolana, K., Khera, A., Mertens, A., Franke, D., Wohlgemuth, K., Dahmer-Heath, M., et al. (2022). Primary URECs: a source to better understand the pathology of renal tubular epithelia in pediatric hereditary cystic kidney diseases. Orphanet J. Rare Dis. *17*, 122. https://doi.org/10.1186/s13023-022-02265-1.
44. Nowak, K.L., and Edelstein, C.L. (2020). Apoptosis and autophagy in polycystic kidney disease (PKD). Cell. Signal. *68*, 109518. https://doi.org/10.1016/j.cellsig.2019.109518.
45. Pavlov, T.S., Levchenko, V., Ilatovskaya, D.V., Palygin, O., and Staruschenko, A. (2015). Impaired epithelial Na+ channel activity contributes to cystogenesis and development of autosomal recessive polycystic kidney disease in PCK rats. Pediatr. Res. *77*, 64–69. https://doi.org/10.1038/pr.2014.145.
46. Ilatovskaya, D.V., Levchenko, V., Pavlov, T.S., Isaeva, E., Klemens, C.A., Johnson, J., Liu, P., Kriegel, A.J., and Staruschenko, A. (2019). Salt-deficient diet exacerbates cystogenesis in ARPKD via epithelial sodium channel (ENaC). EBioMedicine *40*, 663–674. https://doi.org/10.1016/j.ebiom.2019.01.006.
47. Nakanishi, K., Sweeney, W.E., Jr., Zerres, K., Guay-Woodford, L.M., and Avner, E.D. (2000). Proximal tubular cysts in fetal human autosomal recessive polycystic kidney disease. J. Am. Soc. Nephrol. *11*, 760–763. https://doi.org/10.1681/ASN.V114760.
48. Woollard, J.R., Punyashtiti, R., Richardson, S., Masyuk, T.V., Whelan, S., Huang, B.Q., Lager, D.J., vanDeursen, J., Torres, V.E., Gattone, V.H., et al. (2007). A mouse model of autosomal recessive polycystic kidney disease with biliary duct and proximal tubule dilatation. Kidney Int. *72*, 328–336. https://doi.org/10.1038/sj.ki.5002294.
49. Williams, S.S., Cobo-Stark, P., James, L.R., Somlo, S., and Igarashi, P. (2008). Kidney cysts, pancreatic cysts, and biliary disease in a mouse model of autosomal recessive polycystic kidney disease. Pediatr. Nephrol. *23*, 733–741. https://doi.org/10.1007/s00467-007-0735-4.
50. Garcia-Gonzalez, M.A., Menezes, L.F., Piontek, K.B., Kaimori, J., Huso, D.L., Watnick, T., Onuchic, L.F., Guay-Woodford, L.M., and Germino, G.G. (2007). Genetic interaction studies link autosomal dominant and recessive polycystic kidney disease in a common pathway. Hum. Mol. Genet. *16*, 1940–1950. https://doi.org/10.1093/hmg/ddm141.
51. Ransick, A., Lindström, N.O., Liu, J., Zhu, Q., Guo, J.J., Alvarado, G.F., Kim, A.D., Black, H.G., Kim, J., and McMahon, A.P. (2019). Single-Cell Profiling Reveals Sex, Lineage,

and Regional Diversity in the Mouse Kidney. Dev. Cell *51*, 399–413.e7. https://doi.org/10.1016/j.devcel.2019.10.005.

52. Bonventre, J.V., and Yang, L. (2011). Cellular pathophysiology of ischemic acute kidney injury. J. Clin. Invest. *121*, 4210–4221. https://doi.org/10.1172/JCI45161.
53. Schaub, J.A., Venkatachalam, M.A., and Weinberg, J.M. (2021). Proximal Tubular Oxidative Metabolism in Acute Kidney Injury and the Transition to CKD. Kidney360 *2*, 355–364. https://doi.org/10.34067/KID.0004772020.
54. Koenig, H., Goldstone, A., Blume, G., and Lu, C.Y. (1980). Testosterone-mediated sexual dimorphism of mitochondria and lysosomes in mouse kidney proximal tubules. Science *209*, 1023–1026. https://doi.org/10.1126/science.7403864.
55. Yabuki, A., Suzuki, S., Matsumoto, M., and Nishinakagawa, H. (1999). Sexual dimorphism of proximal straight tubular cells in mouse kidney. Anat. Rec. *255*, 316–323. https://doi.org/10.1002/(SICI)1097-0185(19990701)255:3<316::AID-AR7>3.0.CO;2-5.
56. Li, Q.W., Lu, X.Y., You, Y., Sun, H., Liu, X.Y., Ai, J.Z., Tan, R.Z., Chen, T.L., Chen, M.Z., Wang, H.L., et al. (2012). Comparative proteomic analysis suggests that mitochondria are involved in autosomal recessive polycystic kidney disease. Proteomics *12*, 2556–2570. https://doi.org/10.1002/pmic.201100590.
57. Xu, C., Yang, C., Ye, Q., Xu, J., Tong, L., Zhang, Y., Shen, H., Lu, Z., Wang, J., Lai, E., et al. (2021). Mosaic PKHD1 in Polycystic Kidneys Caused Aberrant Protein Expression in the Mitochondria and Lysosomes. Front. Med. *8*, 743150. https://doi.org/10.3389/fmed.2021.743150.
58. Liebau, M.C. (2021). Is There a Functional Role of Mitochondrial Dysfunction in the Pathogenesis of ARPKD? Front. Med. *8*, 739534. https://doi.org/10.3389/fmed.2021.739534.
59. Sansores-Garcia, L., Bossuyt, W., Wada, K.I., Yonemura, S., Tao, C., Sasaki, H., and Halder, G. (2011). Modulating F-actin organization induces organ growth by affecting the Hippo pathway. EMBO J. *30*, 2325–2335. https://doi.org/10.1038/emboj.2011.157.
60. Aragona, M., Panciera, T., Manfrin, A., Giulitti, S., Michielin, F., Elvassore, N., Dupont, S., and Piccolo, S. (2013). A mechanical checkpoint controls multicellular growth through YAP/TAZ regulation by actin-processing factors. Cell *154*, 1047–1059. https://doi.org/10.1016/j.cell.2013.07.042.
61. Hwang, V.J., Kim, J., Rand, A., Yang, C., Sturdivant, S., Hammock, B., Bell, P.D., Guay-Woodford, L.M., and Weiss, R.H. (2015). The cpk model of recessive PKD shows glutamine dependence associated with the production of the oncometabolite 2-hydroxyglutarate. Am. J. Physiol. Renal Physiol. *309*, F492–F498. https://doi.org/10.1152/ajprenal.00238.2015.
62. Chumley, P., Zhou, J., Mrug, S., Chacko, B., Parant, J.M., Challa, A.K., Wilson, L.S., Berryhill, T.F., Barnes, S., Kesterson, R.A., et al. (2019). Truncating PKHD1 and PKD2 mutations alter energy metabolism. Am. J. Physiol. Renal Physiol. *316*, F414–F425. https://doi.org/10.1152/ajprenal.00167.2018.
63. Podrini, C., Cassina, L., and Boletta, A. (2020). Metabolic reprogramming and the role of mitochondria in polycystic kidney disease. Cell. Signal. *67*, 109495. https://doi.org/10.1016/j.cellsig.2019.109495.
64. Gui, Y., Li, J., Lu, Q., Feng, Y., Wang, M., He, W., Yang, J., and Dai, C. (2018). Yap/Taz mediates mTORC2-stimulated fibroblast activation and kidney fibrosis. J. Biol. Chem. *293*, 16364–16375. https://doi.org/10.1074/jbc.RA118.004073.
65. Swenson-Fields, K.I., Vivian, C.J., Salah, S.M., Peda, J.D., Davis, B.M., van Rooijen, N., Wallace, D.P., and Fields, T.A. (2013). Macrophages promote polycystic kidney disease progression. Kidney Int. *83*, 855–864. https://doi.org/10.1038/ki.2012.446.
66. Strubl, S., Torres, J.A., Spindt, A.K., Pellegrini, H., Liebau, M.C., and Weimbs, T. (2020). STAT signaling in polycystic kidney disease. Cell. Signal. *72*, 109639. https://doi.org/10.1016/j.cellsig.2020.109639.
67. Viau, A., Baaziz, M., Aka, A., Mazloum, M., Nguyen, C., Kuehn, E.W., Terzi, F., and Bienaimé, F. (2020). Tubular STAT3 Limits Renal Inflammation in Autosomal Dominant Polycystic Kidney Disease. J. Am. Soc. Nephrol. *31*, 1035–1049. https://doi.org/10.1681/ASN.2019090959.
68. Buchholz, B., Schley, G., Faria, D., Kroening, S., Willam, C., Schreiber, R., Klanke, B., Burzlaff, N., Jantsch, J., Kunzelmann, K., and Eckardt, K.U. (2014). Hypoxia-inducible factor-1alpha causes renal cyst expansion through calcium-activated chloride secretion. J. Am. Soc. Nephrol. *25*, 465–474. https://doi.org/10.1681/ASN.2013030209.
69. Outeda, P., Menezes, L., Hartung, E.A., Bridges, S., Zhou, F., Zhu, X., Xu, H., Huang, Q., Yao, Q., Qian, F., et al. (2017). A novel model of autosomal recessive polycystic kidney questions the role of the fibrocystin C-terminus in disease mechanism. Kidney Int. *92*, 1130–1144. https://doi.org/10.1016/j.kint.2017.04.027.
70. Tesar, V., Ciechanowski, K., Pei, Y., Barash, I., Shannon, M., Li, R., Williams, J.H., Levisetti, M., Arkin, S., and Serra, A. (2017). Bosutinib versus Placebo for Autosomal Dominant Polycystic Kidney Disease. J. Am. Soc. Nephrol. *28*, 3404–3413. https://doi.org/10.1681/ASN.2016111232.
71. Sweeney, W.E., Frost, P., and Avner, E.D. (2017). Tesevatinib ameliorates progression of polycystic kidney disease in rodent models of autosomal recessive polycystic kidney disease. World J. Nephrol. *6*, 188–200. https://doi.org/10.5527/wjn.v6.i4.188.
72. Schneider, C.A., Rasband, W.S., and Eliceiri, K.W. (2012). NIH Image to ImageJ: 25 years of image analysis. Nat. Methods *9*, 671–675. https://doi.org/10.1038/nmeth.2089.

STAR★METHODS

KEY RESOURCES TABLE

REAGENT or RESOURCE	SOURCE	IDENTIFIER
Antibodies		
Mouse monoclonal, Anti-Aquaporin 1, Unconjugated, Clone 1/a5f6	Novus	Cat# NB600-749 RRID: AB_530620
Rabbit polyclonal, Anti-Aquaporin 2	Biorbyt	Cat# orb10123 RRID: AB_10752821
Mouse monoclonal, Anti-CD68 (KP1)	Thermo Fisher Scientific	Cat# 14-0688-82 RRID: 11151139
Rabbit polyclonal, Anti-Cleaved Caspase-3 (Asp175)	Cell Signaling Technology	Cat# 9661 RRID: AB_2341188
Rabbit polyclonal, Anti-Alpha-ENaC	Thermo Fisher Scientific	Cat# PA1-920A RRID: AB_2184369
Rabbit recombinant monoclonal, Anti-F4/80 (D2S9R) XP	Cell Signaling Technology	Cat# 70076 RRID: AB_2799771
Donkey anti-Rabbit IgG (H+L) Cross-Adsorbed polyclonal secondary antibody, Alexa Fluor 488	Thermo Fisher Scientific	Cat# A-21206 RRID: AB_2535792
Donkey anti-Rat IgG (H+L) Cross-Adsorbed polyclonal secondary antibody, Alexa Fluor 488	Thermo Fisher Scientific	Cat# A-21208 RRID: AB_2535794
Goat anti-Mouse IgG (H+L) Cross-Adsorbed polyclonal secondary antibody, Alexa Fluor 555	Thermo Fisher Scientific	Cat #A-21422 RRID: AB_2535844
Goat anti-Rabbit IgG (H+L) Cross-Adsorbed polyclonal secondary antibody, Alexa Fluor 488	Thermo Fisher Scientific	Cat# A-11008 RRID: AB_143165
Goat anti-Rabbit IgG (H+L) Cross-Adsorbed polyclonal secondary antibody, Alexa Fluor 555	Thermo Fisher Scientific	Cat# A-21428 RRID: AB_141784
Goat anti-Rabbit IgG (H+L) polyclonal secondary antibody, HRP	Thermo Fisher Scientific	Cat# A-31460 RRID: AB_228341
IRDye 680RD goat anti-Mouse-IgG, polyclonal	LI-COR Biosciences	Cat# 926-68070 RRID: AB_10956588
IRDye 800CW goat anti-Rabbit IgG, polyclonal	LI-COR Biosciences	Cat# 926-32211 RRID: AB_621843
Rabbit monoclonal, Anti-Ki67	Abcam	Cat# ab16667 RRID: AB_302459
Rabbit polyclonal, Anti-Myosin IIA	Sigma-Aldrich	Cat# M8064 RRID: AB_260673
Rabbit monoclonal, Anti-PCNA (D3H8P) XP	Cell Signaling Technology	Cat# 13110 RRID: AB_2636979
Mouse monoclonal, Anti-Stat3 (124H6)	Cell Signaling Technology	Cat# 9139; RRID: AB_331757
Rabbit monoclonal, Anti-Phospho-Stat3 (Tyr705) (D3A7) XP	Cell Signaling Technology	Cat# 9145 RRID: AB_2491009
Rat monoclonal, Anti-Uromodulin	R&D Systems	Cat# MAB5175 RRID: AB_2890000

(*Continued on next page*)

Continued

REAGENT or RESOURCE	SOURCE	IDENTIFIER
Rabbit monoclonal, Anti-YAP/TAZ (D24E4)	Cell Signaling Technology	Cat# 8418 RRID: AB_10950494
Biological samples		
Kidney sections from *Pkhd1*-knockout (tm/tm), heterozygous (wt/tm) and wildtype (wt/wt) animals	MHH, Department of Pediatric Kidney, Liver and Metabolic Diseases, Hannover, Germany	
Chemicals, peptides, and recombinant proteins		
Direct Red 80	Sigma-Aldrich	Cat# 43665
Hematoxylin	Sigma-Aldrich	Cat# 1.09249.0500
Immunoselect Antifading Mounting Medium DAPI	Dianova/Biozol	Cat# SCR-038448
Intercept (TBS) blocking buffer	LI-COR Biosciences	Cat# 927-60001
Periodic Acid	Sigma-Aldrich	Cat# 1.00524
Protease inhibitor cocktail	Sigma-Aldrich	Cat# P8340
Protran, Amersham	Sigma-Aldrich	Cat# 10600003
Schiffs' Reagent	Sigma-Aldrich	Cat# 3952016
Critical commercial assays		
3,3-Diaminobenzidine (DAB)Metal Enhanced Kit	Thermo Fisher Scientific	Cat# ICN980561 RRID: AB_2335232
BCA Protein Assay Kit	Pierce/Thermo Fisher Scientific	Cat# 23225
PowerTrack SYBR Green Master Mix kit	Thermo Fisher Scientific	Cat# A46113
QuantiTec Reverse Transcription Kit	Qiagen	Cat# 205311
RNeasy Kit	Qiagen	Cat# 74106
TACS 2 TdT-Fluor *In Situ* Apoptosis Detection Kit	R&D Systems	Cat#4812-30-K
Experimental models: Organisms/strains		
C.129(B6-Pkhd1^{tm2Cjwa}/J	The Jackson Laboratory	Cat #021023 RRID: IMSR_JAX:021023
BALB/cJ strain	The Jackson Laboratory	Cat #000651 RRID: IMSR_JAX:000651
Oligonucleotides		
Mouse-Ccl2 Forward: TGGGCCTGCTGTTCACAGTT	Sigma-Aldrich	N/A
Mouse-Ccl2 Reverse: TGGGGCGTTAACTGATCTG	Sigma-Aldrich	N/A
Mouse-C-myc Forward: GGACTGTATGTGGAGCGGTT	Sigma-Aldrich	N/A
Mouse-C-myc Reverse: ACTGAGGGGTCAATGCACTC	Sigma-Aldrich	N/A
Mouse-Col1a2 Forward: TTCTGTGGGTCCTGCTGGGAAA	Sigma-Aldrich	N/A
Mouse-Col1a2 Reverse: TTGTCACCTCGGATGCCTTGAG	Sigma-Aldrich	N/A
Mouse-Ctgf Forward: TGCGAAGCTGACCTGGAGGAAA	Sigma-Aldrich	N/A
Mouse-Ctgf Reverse: CCGCAGAACTTAGCCCTGTATG	Sigma-Aldrich	N/A

(*Continued on next page*)

Continued

REAGENT or RESOURCE	SOURCE	IDENTIFIER
Mouse-Gapdh Forward: TATGTCGTGGAGTCTACTGG	Sigma-Aldrich	N/A
Mouse-Gapdh Reverse: AGTGATGGCATGGACTGTGG	Sigma-Aldrich	N/A
Mouse-Socs3 Forward: GGACCAAGAACCTACGCATCCA	Sigma-Aldrich	N/A
Mouse-Socs3 Reverse: CACCAGCTTGAGTACACAGTCG	Sigma-Aldrich	N/A
Mouse-Stat3 Forward: GCAATACCATTGACCTGCCG	Sigma-Aldrich	N/A
Mouse-Stat3 Reverse: ACGTGAGCGACTCAAACTGC	Sigma-Aldrich	N/A
Mouse-TGFß1 Forward: TTGCTTCAGCTCCACAGAGA	Sigma-Aldrich	N/A
Mouse-TGFß1 Reverse: TGGTTGTAGAGGGCAAGGAC	Sigma-Aldrich	N/A
Software and algorithms		
ImageJ, version 1.53	National Institute of Health	RRID: SCR_003070 https://www.imagej.nih.gov/ij/download.html
GraphPad Prism, version 7.02	GraphPad by Dotmatics	RRID: SCR_002798 https://www.graphpad.com
QuantStudio, version 2.5.0	Life Technologies/ Thermo Fisher Scientific	N/A
Zen 2.6 Zeiss software	ZEISS	N/A
Other		
Zeiss microscope, AxioObserver Z1	ZEISS	RRID: SCR_021351
Axiocam 506	ZEISS	Cat# 426556-0000-000
Axiocam MRc Rev.3 FireWire (D)	ZEISS	Cat# 426508-9902-000
Objective: Plan-Apochromat 20x/0.8	ZEISS	Cat# 440640-9903-000
Cobas C111 analyzer	Roche Diagnostics	Cat# 04528778001
Odyssey Fc Imaging System	LICOR Biosciences	RRID: SCR_023227
QuantStudio 6 Pro	Life Technologies/ Thermo Fisher Scientific	Cat# A43161 RRID: SCR_020239
Standard rodent chow, TPF1324	Altromin	Cat# 1324
TissueLyser LT	Qiagen	Cat# 85600 RRID: SCR_020428

RESOURCE AVAILABILITY

Lead contact

- Further information and requests for resources and reagents should be directed to and will be fulfilled by the lead contact, Wolfgang Ziegler (Ziegler.Wolfgang@mh-hannover.de)

Materials availability

- Our study did not generate new unique reagents.

Data and code availability

- All data reported in this paper will be shared by the lead contact upon request.

- This paper does not report original code.
- Any additional information required to reanalyze the data reported in this paper is available from the lead contact upon request.

EXPERIMENTAL MODEL AND STUDY PARTICIPANT DETAILS

Animals

All mice were maintained in the Hannover Medical School Specific-Pathogen-Free (SPF) Animal Facility Unit. The following *Pkhd1*-knockout transgenic mouse line was used: C.129(B6)-*Pkhd1*^{tm2Cjwa}/J, generated in the laboratory of Christopher Ward.[31] Mice were provided by The Jackson Laboratory, Bar Harbor, MA, USA as JAX stock #021023, which is backcrossed to the BALB/cJ strain (JAX stock #000651). The *Pkhd1*-knockout was achieved by targeted mutation of intron 2 inserting a loxP-STOP-loxP (LSL) cassette, containing a puromycin acetyl transferase (pac) gene and four copies of an SV40 viral transcriptional termination sequence, that terminates all *Pkhd1* transcripts in intron 2. Breeding, husbandry and handling of animals was performed according to approved animal protocols. Due to the mild kidney phenotype of male homozygous *Pkhd1* (tm/tm) knockout mice,[31] cystic kidney disease was analyzed only in female animals. Mice on standard rodent chow, TPF 1324 (Altromin Spezialfutter, Lage, Germany) were kept in mixed genetic groups of homozygous *Pkhd1* (tm/tm) knockout and control animals, heterozygous *Pkhd1* (wt/tm) or wildtype *Pkhd1* (wt/wt). Animal well-being and health status, including weight, were monitored regularly.

Study approval

The animal study was approved by the Niedersächsisches Landesamt für Verbraucherschutz und Lebensmittelsicherheit (LAVES), Oldenburg, Germany (Authorization number: Az 19/3103).

METHOD DETAILS

Section preparation, immunofluorescence, immunohistochemistry

At 3, 6 and 9 months of age, the animals were euthanized with prior collection of urine and blood samples and dissected. Serum, plasma, and urine samples were collected and stored at -80°C. Organs were snap frozen or processed for paraffin embedding. To allow comparison of organ weights among different genotypes and ages, relative organ weights were calculated using total body weight at the time of selection. After fixation in 4% paraformaldehyde, kidneys were embedded in paraffin blocks and cut to 2.5 µm sections. Tissue sections were deparaffinized, and stained with hematoxylin (#1.09249.0500) and PAS (Periodic Acid, #1.00524; Schiffs' Reagent, #3952016), all from Sigma-Aldrich, Taufkirchen, Germany. Picro-Sirius Red staining was performed according to provider's protocols (Direct Red 80; #43665, Sigma-Aldrich). TUNEL staining was performed using the TACS 2 TdT-Fluor *In Situ* Apoptosis Detection Kit (#4812-30-K, R & D Systems) according to provider's protocol.

Immunofluorescence: sections were blocked with normal goat (or donkey) serum in PBS and washed with either PBS or TBST. Primary antibodies were incubated at 4°C overnight and secondary antisera for 1h, with dilutions according to manufacturers' recommendation. DAPI mounting medium (#SCR-038448; Dianova / Biozol, Hamburg, Germany) was used to stain nuclei. Primary antibodies used were, Alpha-ENaC (#PA1-920A, Thermo Fisher Scientific, Waltam, MA, USA), Aquaporin1 (#NB6009471; Novusbio, Abingdon, United Kingdom), Aquaporin 2 (#10123; Biorbyt, Cambridge, United Kingdom), CD68 (KP1) (#14-0688-82, Thermo Fisher Scientific), Cleaved Caspase-3 (Asp175) (#9661; Cell Signaling Technology, Frankfurt, Germany), Ki67 (#ab166671; Abcam, Cambridge, United Kingdom), PCNA (D3H8P) (#13110, Cell Signaling Technology), mUromodulin (#MAB5175; R&D Systems, Minneapolis, MN, USA), YAP/TAZ (#8418; Cell Signaling Technology) and secondary antisera, Alexa Fluor 488 goat anti-rabbit IgG (#A-11008), Alexa Fluor 488 donkey anti-rat IgG (#A-21208), Alexa Fluor 488 donkey anti-rabbit (#A-21206), Alexa Fluor 555 goat anti-rabbit IgG (#A-21428), and Alexa Fluor 555 goat anti-mouse IgG (#A-21422), all from Thermo Fisher Scientific.

Immunohistochemistry: Slices were deparaffinized with xylol and series of grading alcohols. Antigen retrieval was performed using citrate buffer followed by 3% peroxidase blocking with H_2O_2. After blocking and rehydration, primary antibodies were incubated at 4°C overnight, secondary antiserum for 1h. Afterwards, an incubation with Metal Enhanced DAB Substrate Kit (#ICN980561; Thermo Fisher Scientific) followed to visualize the antibody complexes. Nuclei were counterstained with hematoxylin. Stained sections were mounted in Roti-Mounting medium (HP 68.1; Carl Roth, Karlsruhe, Germany). Antibodies were F-4/80 (#70076) and Phospho-STAT3 (Tyr705) (#9145), both Cell Signaling Technology, Frankfurt, Germany, and Peroxidase-conjugated AffiniPure Goat Anti-Rabbit IgG (#31460; Thermo Fisher Scientific).

Microscopy and quantitative image analysis

Images of cross sections were acquired on the Zeiss AxioObserver Z1 microscope, using 20x Plan-Apochromat (NA 0.8) objective and AxioCam MRc Rev.3 for color imaging, or illumination with Colibri 7 and Axiocam 506 mono for fluorescence imaging. Software package Zen 2.6 was used to control image acquisition and assembly of overviews (all from Zeiss, Göttingen, Germany). Filter sets and related staining were as follows: (1) Alexa Fluor 488 - filter set 38 HE, (2) Alexa *Fluor 555 - filter set 43 HE, and (3) DAPI - filter set 49 (all filter sets from Zeiss).*

Cyst formation, Cystic Index: Cross sections of kidney tissue were stained with hematoxylin-PAS (H-PAS) and overview images of entire cross sections collected using the Zeiss Axio Observer. Detection of cysts and quantification of cyst numbers and cystic areas was performed in ImageJ software, version 1.53,[72] see Figure S1C. Software tools are indicated by <*Name*>. In brief, following import of individual overview images, cortex area was defined using <*freehand*> and area determined in [μm^2] by <*measure*>. Then, image was converted to 8-bit and inverted. After enhancing contrast, a binary mask was created, and the threshold for cystic tubules set to diameters $\geq$ 50µm. <*analyze particles*> generated a mask showing automatically recognized cysts, and furthermore, determined (i) total number of cysts, (ii) cystic area in [μm^2] and (iii) average size of cysts in [μm^2]. In this mask, automatically marked areas were evaluated manually, and vascular lumina and artifacts removed with <*freehand*> to correct cyst number and cystic area. The edited mask was re-analyzed using <*analyze particles*>. Total cystic area was set off against total cortex area to determine Cystic Index [% cyst area / cortex area].

Fibrosis, Fibrotic Index: Fibrotic remodeling in kidney tissue was assessed using Picro-Sirius Red (SR) staining. Overview images of entire cross sections were collected using the Zeiss Axio Observer and analyzed by ImageJ, see Figure S1D. In brief, following import of individual overview images, cortex area was defined using <*freehand*> and area determined in [μm^2] by <*measure*>. Image was converted to RGB. Veins, arteries and glomeruli were removed manually with <*freehand*> to disregard physiological occurrence of collagen fibers. In the green channel, threshold was set to only score collagen fibers and fibrotic area determined in [μm^2] using <*measure*>. Total fibrotic area was set off against total cortex area to determine Fibrotic Index [% fibrotic area / cortex area].

Macrophages, F4/80, and CD68 co-staining: Inflammation processes were evaluated by measuring the area of macrophages in relation to the total area of kidney tissue per field [% F4/80 area/cortex area], using ImageJ. The analysis was based on five fields of the corticomedullary border for each animal, building an average value. Incidence of CD68 / F4/80 double positive M1 macrophages was determined by analyzing five randomly chosen fields within the corticomedullary border. In each field, five F4/80-positive areas were marked. Using ZEN2.6 imaging software, these areas were assessed for CD68 co-staining. Thus 25 areas per animal were used to calculate the proportion of M1 to total number of macrophages.

Proliferation, Ki67 and PCNA: Five randomly chosen fields of the corticomedullary border were analyzed for each animal. The overall number of nuclei per field was counted automatically using ImageJ. Fluorescence channels were split to allow count of Ki67 or PCNA-positive nuclei. Mean value of Ki67 / PCNA- expressing nuclei in relation to all nuclei was calculated for each animal.

Apoptosis, Caspase-3(Casp3): Apoptotic processes in kidney tissue were addressed based on cleaved Casp3 stained overview images. Total number of cysts, defined as tubules with diameters $\geq$ 50µm, was determined automatically by creating a binary mask of overviews using ImageJ (see cyst formation). Lumina with Casp3-positive cells and cell detritus were counted to calculate percentage of Casp3-positive to all cystic lumina [% Casp3 positive / all lumina].

Transcriptional regulators, pSTAT3, YAP/TAZ: To determine nuclear localization of pSTAT3 and YAP/TAZ, five random fields of the corticomedullary border for each animal were analyzed using ImageJ. In each field, either five cystic tubules in *Pkhd1*-knockout or five non-dilated tubules (cystic not available) in control animals were randomly selected and circled. Epithelial nuclei were counted automatically, and nuclei expressing pSTAT3 or YAP/TAZ identified by hand. Average rate of epithelial nuclei showing nuclear localization of transcriptional regulators was calculated based on 25 tubules per animal [% pos. nuclei / epith. nuclei].

Western Blot

Kidney tissue was extracted in RIPA buffer, 50mM Tris-HCl (pH 7.4), 1% Triton-x-100, 0.25% Na-deoxycholate, 200mM NaCl, 1mM EDTA, protease inhibitor cocktail (#P8340; Sigma-Aldrich), 1mM Na3VO4 (1:200), 1mM NaF (1:200), using TissueLyser LT (Qiagen; Hilden, Germany). Total protein contend was determined with BCA Protein Assay Kit (#23225; Pierce / Thermo Fisher Scientific). Total kidney lysates, 35µg per lane were separated on 10% SDS-PAGE gels using Tris/glycine buffer. After transfer onto nitrocellulose membrane, Amersham Protran (#10600003; Sigma-Aldrich), membranes were blocked using 5% BSA in TBST with 50% (v/v) Intercept (TBS) blocking buffer (#927-60001; LI-COR Biosciences, Bad Homburg, Germany) and developed using primary antisera, phospho-STAT3 (Tyr705) (D3A7) (#9145), STAT3 (124H6) (#9139), both from Cell Signaling Technology, and myosin IIA (#M8064; Sigma-Aldrich). Secondary antisera used were, IRDye 800CW goat anti-rabbit-IgG (#926-32211), IRDye 680RD goat anti-mouse-IgG (#926-68070) and protein band intensities quantified based on fluorescence detection using the Odyssey Fc Imaging System, all from LI-COR Biosciences.

Quantification of gene expression

Using realtime PCR, transcription of genes, *Ccl2, c-Myc, Col1a2, Ctgf, Socs3, Stat3,* and *Tgf-b*, was determined in relation to a house keeping gene, *Gapdh*, and expression levels calculated using $2^{-\Delta\Delta Ct}$ values. Kidney tissue was homogenized using 5mm stainless steel beads (#69989) and TissueLyser LT (#85600), all from Qiagen, Helden, Germany. Total RNA was extracted from the homogenates using RNeasy Kit (#74106, Qiagen), following manufacturer's instructions. RNA, 500ng per each tissue homogenate, was transcribed into cDNA using QuantiTect Reverse Transcription kit (#205311, Qiagen). Gene expression was determined in triplicates using PowerTrack SYBR Green Master Mix kit (#A46113, Thermo Fisher Scientific) and the QuantStudio 6 Pro instrument (#A43161, Thermo Fisher Scientific) for realtime PCR. Data were analyzed using the QuantStudio design and analysis software version 2.5.0. Primer sequences are shown in the key resources table, primer specificity was ensured by determining DNA melting curves.

QUANTIFICATION AND STATISTICAL ANALYSIS

Since there was no prior information available, with respect to the frequency and extent of cyst development in *Pkhd1* knockout mice with BALB/cJ background, the group size of 8 animals per genotype was establish during this study. The groups of 9-months old mice were extended to 9 animals each, to avoid selection of available knockout females in the litters. Data are reported as mean ± SD. Data sets were tested for normality and differences among groups evaluated using Two-way analysis of variance (ANOVA) followed by Tukey's multiple comparison. For nonparametric analyses, Mann-Whitney was used as indicated. $P < 0.05$ was accepted as statistical significance. All tests were performed using GraphPad Prism version 7.02 or later; GraphPad Software, San Diego, CA, USA.